AMERICAN UNIVERSITY OF BEIRUT

LIQUID PHASE KETONIZATION OF PENTANOIC ACID INTO 5-NONANONE

by
ELISE ELIAS FARAH

A thesis
submitted in partial fulfillment of the requirements
for the degree of Master of Sciences
to the Department of Chemical and Petroleum Engineering
of the Faculty of Engineering and Architecture
at the American University of Beirut

Beirut, Lebanon
May 2018

AMERICAN UNIVERSITY OF BEIRUT

LIQUID PHASE KETONIZATION OF PENTANOIC ACID INTO 5-NONANONE

by

ELISE ELIAS FARAH

Approved by:

Belal Abu Tarboush
on behalf of Dr. Ahmad

Dr. Mohamad Ahmad, Professor, Chairman — Advisor
Department of Chemical and Petroleum Engineering

Dr. Belal Abu Tarboush, Assistant Professor — Member of Committee
Department of Chemical and Petroleum Engineering

Dr. Mu'tasem Shehadeh, Associate Professor — Member of Committee
Department of Mechanical Engineering

Date of thesis defense: May 2, 2018

AMERICAN UNIVERSITY OF BEIRUT

THESIS, DISSERTATION, PROJECT RELEASE FORM

Student Name: FARAH ELISE ELIAS

Last First Middle

● Master's Thesis ○ Master's Project ○ Doctoral Dissertation

☐ I authorize the American University of Beirut to: (a) reproduce hard or electronic copies of my thesis, dissertation, or project; (b) include such copies in the archives and digital repositories of the University; and (c) make freely available such copies to third parties for research or educational purposes.

☑ I authorize the American University of Beirut, to: (a) reproduce hard or electronic copies of it; (b) include such copies in the archives and digital repositories of the University; and (c) make freely available such copies to third parties for research or educational purposes after:

One ---- year from the date of submission of my thesis.
Two ---- years from the date of submission of my thesis.
Three --✓-- years from the date of submission of my thesis.

Signature May 10, 2018

Date

ACKNOWLEDGMENTS

AN ABSTRACT OF THE THESIS OF

Elise Elias Farah for Master of Science
Major: Chemical and Petroleum Engineering

Title: Liquid Phase Ketonization of Pentanoic Acid into 5-Nonanone

The world's energy consumption is increasing at a high rate due to the expansion of the world's population, especially in third world countries. The demand in energy is far exceeding the supply capability, and the available sources of energy are leaning towards depletion, which was the main cause for the development of alternative sources of energy such as wind energy, solar energy, hydro fuel cells and many others. However, the transportation sector remains highly dependent on liquid carbon fuels, which resulted in extensive researches to find an alternative way to produce them in a clean renewable process. The conversion of raw material, such as biomass, into high value chemicals is considered a promising trend in the field. Biomass can be cracked through a well designed process to produce pentanoic acid, which is further converted to 5-nonanone, hydrogenated to nonane, key precursor for biofuel. This process is called ketonization, and although vapor and organic phases ketonization are the most adopted, liquid phase ketonization shows higher advantages such as lower operating temperatures and enhanced conversion efficiency. In this work, liquid phase ketonization of pentanoic acid was tested in a batch reactor under a temperature of 350 °C and a pressure of 30 bar, using $CeZrO_2$ and ZrO_2 at different calcination temperatures as catalysts. The catalysts were characterized using XRD to study the crystallinity of the catalysts, BET to determine their surface area and pore sizes, SEM to familiarize with their structure, TGA to check their stability and XPS to depict any changes on the surface between the catalysts, and they were later tested for this experiment. The experiment turned out to be feasible using ZrO_2 calcined at 400 °C, while the other catalysts were unsuccessful.

CONTENTS

ILLUSTRATIONS

Figure Page

TABLES

CHAPTER I

INTRODUCTION

In a research case conducted by the International Energy Outlook 2017, a projection of the evolution of the world energy consumption is clearly represented as an increase of 28% between 2015 and 2040. This increase results mainly from the non-OECD (Organization for Economic Cooperation and Development) countries, contributing more than 41% compared to 9% related to the OECD countries [1]. Energy consumption will increase from 575 quadrillion BTU (British thermal units) in 2020, to more than 700 quadrillion BTU in 2040. The main reason for this increase leads back to the growth of the world population mainly in Asia (China and India), and to the variation of the oil price depending on the supply and demand of liquid fuel. The consumption of liquid fuel is partitioned into four different sectors: transportation, industry, buildings and construction, and electricity. While electrical consumption is expected to be decreased by 2% between 2015 and 2040, this saving will be compensated by the transportation sector, where the consumption is expected to increase due to the expansion in population and their demand for more fuel. Therefore, the general trend of liquid fuel consumption will continue to increase slowly, consequently the available sources of energy will be facing a severe depletion. Finding an alternative source of energy has become very crucial to overcome the growing gap between the demands and the supplies [1]. On the other hand, the combustion of the fuel generates huge quantities of CO_2 released into the environment, contributing to the rise of the environmental concern [2]. To mitigate the effect of CO_2 release, biofuels are

being adopted as alternative safe source of energy. Research in this field pointed to many renewable sources such as lignocellulosic biomass. Biomass is considered a clean and cheap source of energy, and it is available at all time. Biomass is decomposed through heating to cellulose, hemicellulose and lignin. Each of these compounds is converted to another product used in specialty and commodity chemicals, herbicides and pesticides, heating oil and transportation fuels [3]. More specifically, cellulose is broken into sugars, which can be converted into HMF or hydroxymethyl furfural which is then fractured into formic acid and levulinic acid. The latter acid is converted into valeric acid while the former acid generates CO_2 and H_2 that is used as a medium for the conversion of the valeric acid into 5-nonanone through a process called “ketonization”. The final product of the scheme, upon hydrogenation, is transformed into nonane, a biofuel additive. Ketonization converts the carboxylic acids into ketones with the release of CO_2 and water in presence of a catalyst, usually metal oxides. The presence of oxygen in biofuel is proved to reduce its heating value, favoring the use of available petroleum sources. Therefore, the main advantage of the acid treatment through ketonization is the obstruction of the high reactivity of these acids by elongating their short chain length into a longer one with a lower oxygen content as well. The longer chain ketones are usually used in medical field in acne treatment and peeling, in the production and the dissolution of plastics and synthetic fibers, in paints, and lately as a precursor for gasoline and diesel, considered as biofuel, through dehydrogenation into an alkane form characterized by a high lubricity, stability and a good cetane number.

CHAPTER II

LITERATURE REVIEW AND THEORETICAL BACKGROUND

A. Ketonization reaction

Decarboxylation, or more specifically ketonic decarboxylation, is the reaction of ketonization of carboxylic acids to synthesize symmetric and asymmetric ketones. The reaction of ketonization is as follows (Eq. 1) [4].

$$R_1COOH + R_2COOH \rightarrow R_1COR_2 + CO_2 + H_2O \quad \text{Eq. 1}$$

Ketonization is the reaction that converts a low carbon chain with two oxygen atoms to a higher carbon chain with one oxygen atom, which increases the stability of the hydrocarbon and its energy content [4]. The ketonic decarboxylation can take place in gaseous phase, organic phase or aqueous phase. In the gaseous phase, all reactants and products are gases, the temperature is elevated enough to vaporize the materials. The organic and aqueous phases are similar in concept; the acid is mixed with hexane or water and the reaction proceeds without any phase changes observed. Two possible reactions exist: homo-ketonization and cross-ketonization. In the first case, two molecules of the same carboxylic acids react together to produce a symmetric ketone, along with water and carbon dioxide. For example, the reaction between two acetic acids would generate acetone as shown in Eq. 2

$$2\,CH_3COOH \rightarrow CH_3COCH_3 + H_2O + CO_2 \quad \text{Eq. 2}$$

The cross-ketonization is the reaction that results in the formation of three ketones in addition to the carbon dioxide and the water. This reaction takes place between two different carboxylic acids and generates two symmetric ketones and one asymmetric

ketone [5]. The ketones obtained can be further processed through aldol condensation to produce saturated hydrocarbons, perfect candidates for bio-fuel and bio-diesel preparation [4]. Three conditions are known to be applied in this reaction, which are pyrolytic, catalytic and photolytic conditions. However, due to its simplicity, its versatility, its ease of application, and its cost, the catalytic route is the most adopted [6]. Three types of decarboxylation exist in organic chemistry, which are the reductive decarboxylation that results in an aromatic hydrocarbon, the ketonic decarboxylation that yields a ketone, and the oxidative decarboxylation. However, metal oxides are widely known to be selective for the ketonic decarboxylation. They can be classified into low lattice energy oxides such as CaO, MgO, BaO, etc. and into high lattice energy oxides such as ZrO_2, TiO_2, Al_2O_3 and many others. Both categories provide different pathways for the ketonization of the acids, which will be discussed in the next section [4].

B. Ketonization mechanism

1. Surface and bulk ketonization

The most important factor that affects the mechanism of the reaction is the lattice energy of the catalyst used. As mentioned in "Ketonization of Carboxylic Acids: Mechanisms, Catalysts, and Implications for Biomass Conversion" (2013) [4], the low lattice energy catalysts favor the bulk ketonization, whereas the high lattice energy oxides direct towards the surface ketonization.

The difference between the two phenomena remains in the intermediates formed throughout the reaction. The bulk ketonization refers to the formation of a bulk

carboxylate salt, which will be later decomposed into ketone, carbon dioxide and water, the case in which the catalyst reacts strongly with the acid. High lattice energy oxides are limited to a reaction at their surface only. Another remarkable difference between these two types of catalyst is the rate of disappearance of the reactants and the rate of formation of the product. Using high lattice oxides, the rates occur simultaneously, the reactants deplete as the products are formed; which is not true for the low lattice energy oxides where the concentration of the acid decreases before any of the products is formed [4].

2. α-Hydrogen mechanism

For the ketonization reaction to take place, one carboxylic acid at least should carry an α-hydrogen. For the sake of the explanation, an α-hydrogen is the hydrogen linked to the carbon located right next to the carbonyl group. This specific hydrogen has particular characteristics, one of which is the higher acidity than the other hydrogen atoms in the molecule [4]. For example, any alkyl C-H bond dissociation requires typically a pK_a value ranging between 40 and 50, whereas an α-hydrogen atom require a value of 19 to 20 [7]. As a result, the activity of the reaction is highly dependent on the number of α-hydrogen atoms carried by the acid.

Neunhoeffer and Paschke first realized the essential role of these atoms [8] in the ketonization reaction of the adipic acid into cyclopentanone. They also illustrated a mechanism that explains the reaction: the basic site of the catalyst attracts the α-hydrogen creating a nucleophilic site on the carboxylic acid. This site then attacks the other acid to create the ketone.

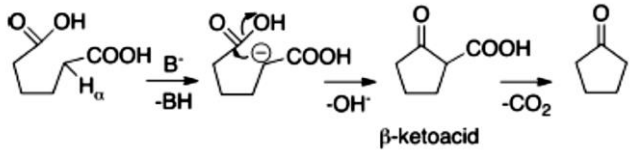

Figure 1: The mechanism proposed by Neunhoeffer and Paschke [8]

Ponec et al. [9] further studied the proposed mechanism and came up with the conclusion that the rate of the ketone formation was proportional to the number of α-hydrogens present on the carboxylic acids. Nagashima et al. [10] confirmed the previous work by reacting multiple acids such as propanoic acid, 2-methylpropanoic acid, 2,2-dimethylpropanoic acid and others having different number of α-hydrogens. They came up with the same conclusion that states that the higher the number of α-hydrogens, the higher the rate of formation of the ketone, and this is applicable for both self- and cross-ketonizations. However, their work lightened on another factor influencing the reactivity of the reaction, which is the number of substituents at the β-position. It goes as follows: the higher the number of the substituents at the β-position, the lower is the reactivity of the reaction. Pulido at al.'s work emphasized on the importance of the hydrogen atoms on at least one of the acids. They studied the self- and cross-ketonization of pivalic acid having no α-hydrogens and valeric acid with α-hydrogen atoms, resulting in a high conversion of the valeric acid and the absence of conversion of the pivalic acid in the self-ketonization and a very low conversion in the cross-ketonization [5]. Ignatchenko [11] proposed the study of the energy needed for the abstraction of the α-hydrogen, which turned out to be 120-159 kJ/mol, whereas Pulido et al. [5] compared two mechanisms, one involving the abstraction of the α-hydrogen and one that doesn't. They found that the activation energy of the former mechanism

was lower than that of the latter one, which favours the α-hydrogen mechanism proposed. The detachment of the α-hydrogen creates a reactive nucleophile that readily attacks the other acid molecule, forming a β-ketoacid (a mechanism that will be later discussed) easily decarboxylated into a ketone. It is also important to mention that a competition between the decarboxylation of the β-ketoacid and the protonation of the dianion. Another function of the α-hydrogen in the ketonization without the formation of the dianion by elimination exists [12]. The intramolecular transfer of the α-hydrogen would initiate a keto-enol tautomerization reaction as shown in Fig. 2.

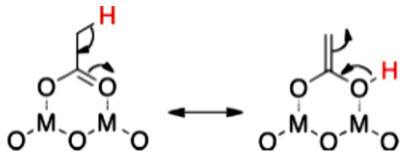

Figure 2: Conversion of the carboxylate into ketone by keto-enol tautomerization [12]

Calculations concerning these two routes are still missing; no path is known to be more favorable than the other is. Despite the lack of information related to the ketonization and to the involvement of the α-hydrogen in the mechanism, the importance of this atom is non-debatable since it is considered the foundation of the suggested mechanisms discussed in the following sections [4].

3. Ketene formation

Ketenes are organic compounds that result from the dehydration of an α-hydrogen of a carboxylic acid. Their chemical formula is R-C=C=O [13]. It is considered as an intermediate in the ketonization reaction due to the necessity of an α-hydrogen. The first mechanism involving a ketene formation was proposed by Munuera et al. [14] in 1978

and confirmed by Dooley et al. [15-17]. It summarizes as follows: the metal surface deprotonates the acid resulting in a carboxylate molecule that dehydrates into a ketene. The ketene will then attack another carboxylate molecule and the ketone is formed in which the acyl group derives from the ketene molecule. A representation of the mechanism is exemplified in Fig. 3

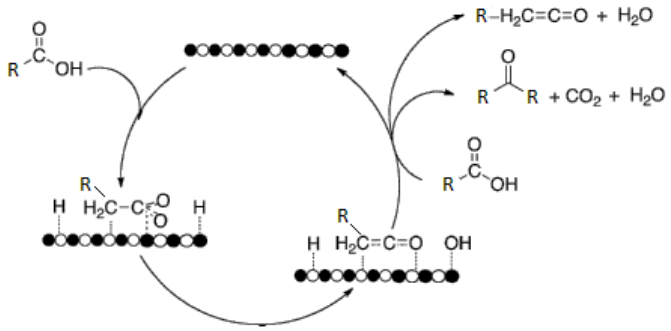

Figure 3: Ketonic decarboxylation based on ketene formation [14]

As previously mentioned, Munuera et al. [14] employed the FT-IR to analyse the intermediates during the ketonization of acetic acid on TiO_2 surface. An analogy was found between the absorption bands of the vapour phase ketene ranging between 3005 and 1730 cm^{-1} and the bands detected on the FT-IR, which proved the existence of the ketene intermediate. Another proof would be the development temperature of the acetone which matched exactly the disappearance temperature of the ketene. Moreover, Dooley et al. [15-17] sustained the ketene formation by conducting the ketonization of acetic acid containing deuterium atoms at the α-position and cyclopropane carboxylic acid with hydrogen atoms using cerium dioxide and titanium dioxide combined catalyst under different conditions. They were able to confirm that the α-hydrogen was involved

in the mechanism and that no other mechanism was observed. However, these results do not demonstrate the involvement of the ketene intermediate in the ketonization reaction. Regardless of the above theories and demonstrations, the coupling process occurring between the ketene and the carboxylate is still missing many details, since no organic chemistry mechanism goes down to one-step only [18]. Therefore, the only support of this mechanism would be the need of the α-hydrogen. Some suggested opposing points of view. The main counter-argument ensues from Ponec at al. [19] that explains the presence of ketene as a side product rather than an intermediate. They reacted pivalic acid deprived of any α-hydrogen with acetic acid having a ^{13}C in the acyl group to track the exchange of the groups during the ketone formation. The result was the formation of 2,2-dimethyl-3-butanone having no ^{13}C (that can only come from the acetic acid) and the release of CO_2 all labelled with ^{13}C. Consequently, the carbonyl group in the ketone originates from the pivalic acid, whereas the CO_2 derives from the acetic acid. Since the pivalic acid has no α-hydrogen, the ketene formation as an intermediate is not a valid mechanism in this case, the only explanation of the presence of the ketene would be that it is considered as side product. Conducting similar experiments, Martinez and Barteau [20] came up with the same conclusion that excludes the possibility of sequential reaction between ketene and ketone but confirms the occurrence of their parallel reactions [21].

4. β-ketoacid formation

As previously discussed, the α-hydrogen plays a paramount role in the ketonization reaction; however, the concept of an α-hydrogen does not mention any intermediate that facilitates the coupling process at the surface of the catalyst. The notion of a β-ketoacid

then emerged as the ideal intermediate that satisfies the conditions of the ketonization. A β-ketoacid is a result of combining an enolate and a carboxylate, which contains a carbonyl group at the β-position of the acid; it is also referred to as 3-oxocarboxylic acid. Upon decarboxylation in a mild thermal environment, the β-ketoacid is then converted to a ketone with a release of a carbon dioxide molecule [4]. The decarboxylation is generally easy to occur, and it generates an enol, outcome of the "redistribution of six electrons in a six-membered cyclic transition state", which tautomerizes into the corresponding ketone [22].

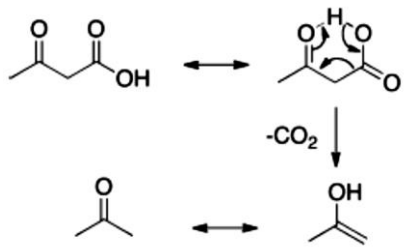

Figure 4: Decarboxylation and tautomerization of a β-ketoacid [22]

Neunhoeffer and Paschke [8] originally pointed to its role while studying the ketonization of adipic acid (review Fig.1) to produce cyclopentanone. Few studies have been made to confirm the presence of the β-ketoacid intermediate during the ketonic decarboxylation. However, the decarboxylation of the intermediate occurs instantly as it is formed, which hinders its detection. Nagashima et al. [10] explained the above mechanism in the figure below.

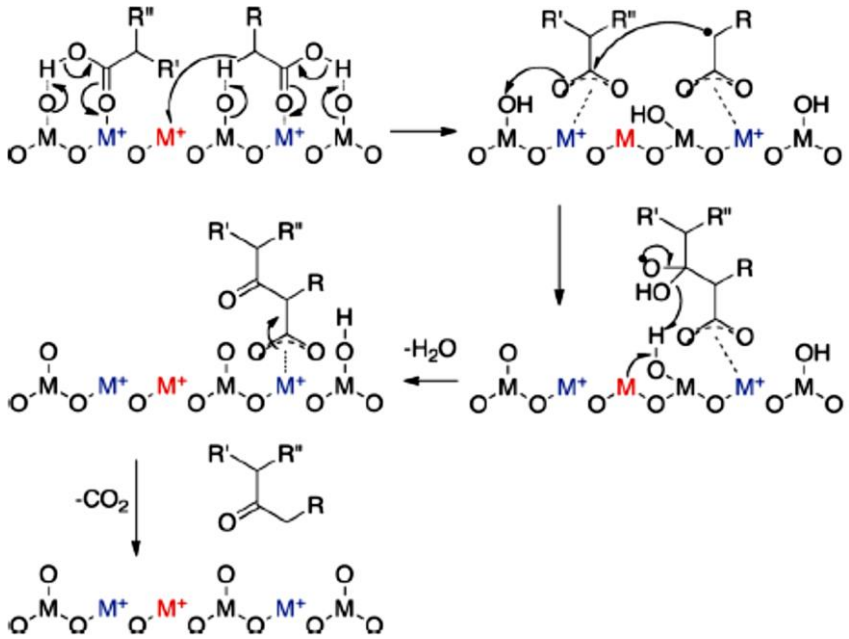

Figure 5: The β-ketoacid mechanism as explained by Nagashima et al.[10]

First, the metal surface provokes the formation of carboxylates. An α-hydrogen atom is subtracted from the carboxylate, reducing it to an anionic radical that subsequently attacks the other carboxylate, forming the β-ketoacid that further decarboxylates into a ketone.

Pham et al. [12] elaborated another ketonization route shown in Fig.6 below. The two routes are very similar; however, in the latter one, the carboxylic acid is transformed to an enol, which requires less energy than the deprotonation of the α-hydrogen. The β-ketoacid then evolves from the nucleophilic attack of the enolized carboxylate on the other carboxylate molecule. It next decomposes to a ketone and a CO_2 molecule. It is important to mention that both routes account for the necessity of the α-hydrogen to form the β-ketoacid; it is either subtracted by the surface of the catalyst or removed through enolization.

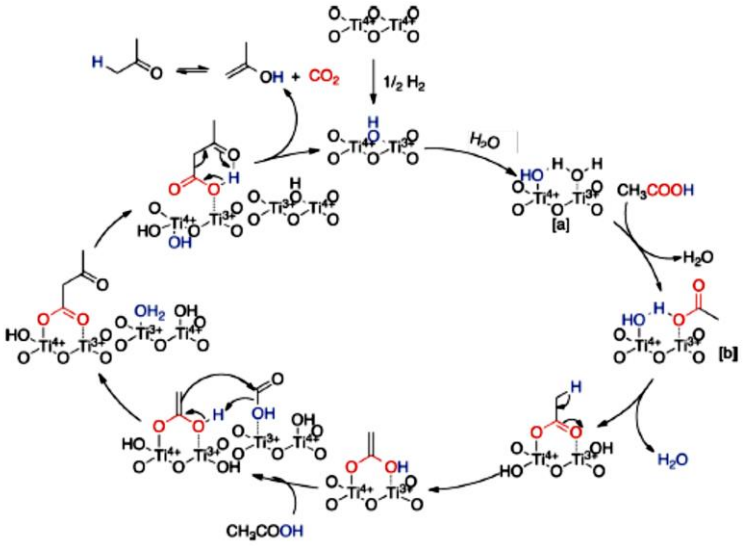

Figure 6: The formation of β-ketoacid as proposed by Pham et al. [12]

The above explanation is compatible with the conclusion deduced by Ponec et al. [19] and discussed previously. For the sake of the clarification, they concluded that the molecule of CO_2 derives from the carboxylate deprived from its α-hydrogen. Similarly, the β-ketoacid emanates from the decarboxylated carboxylate that previously encounters an enolization or an α-hydrogen removal [4]. Nevertheless, in the mechanisms already explained, the β-ketoacid results from the coupling of two adjoining carboxylates; however, Renz et al. [5] and Ignatchenko et al. [23] stated that the β-ketoacid is formed by an enolate (a carboxylic acid that has undergone a deprotonation and an α-hydrogen removal) and an acylium ion (a carboxylic acid that has lost its –OH group) [24, 25]. Renz et al. [5] assembled the mechanism as follows.

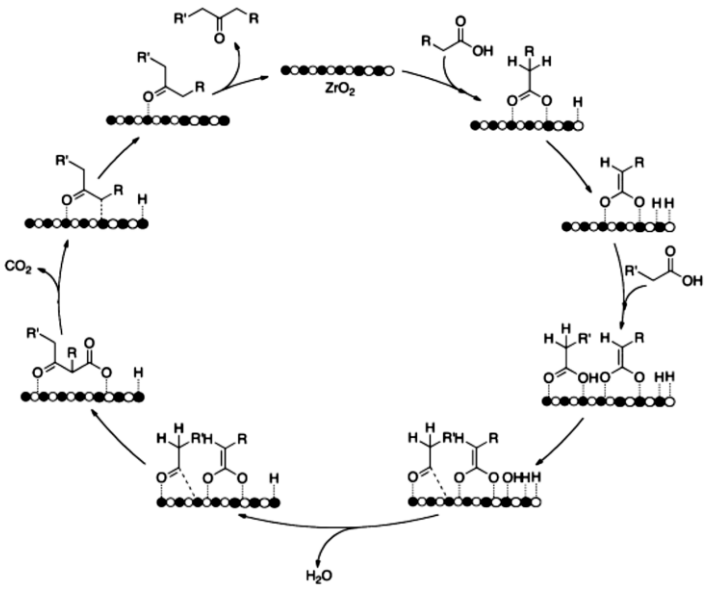

Figure 7: The ketonization mechanism through β-ketoacid evolution from acylium ion and enolate as suggested by Renz et al. [5]

Pulido et al. [5] evaluated the energy barriers required for each of the routes, and came with the conclusion that the β-ketoacid mechanism demands lower energy than the other paths. They weakened the credibility of their calculations by stating that the rate-determining step is that of the β-ketoacid decarboxylation, which is inconsistent with the consensus that the decarboxylation step is generally easy and instant by thermal treatment.

5. Other mechanisms

The proposed mechanisms are not limited to the α-hydrogen, ketene formation and β-ketoacid intermediate. Other mechanisms have been proposed; the generation of methylene as intermediate observed by Ponec et al.[26], a hypothesis rejected by Nagashima et al. [10] who argue that this intermediate should react with water and form methanol. Another theory would be the formation of acid anhydride as intermediate, a

mechanism suggested by Bamberger [27].This anhydride is believed to derive from the coupling of a ketene and a carboxylic acid and it later decarboxylates into a ketone.

C. Gaseous Phase Ketonization of Pentanoic Acid

The gaseous phase ketonization consists of the conversion of valeric acid into 5-nonanone under elevated temperatures and atmospheric pressure. Zaytseva, et al. (2013) compared three catalysts which are ZrO_2, CeO_2 and (5-20%) CeO_2-ZrO_2. They found that the highest conversion was recorded using 10% CeO_2-ZrO_2 and ZrO_2, while the lowest conversion was obtained using the CeO_2 catalyst. Moreover, the reaction taking place under H_2 medium resulted in a higher conversion than that in N_2 medium, concluding that this reaction is highly dependent on the Lewis acid sites [28]. Another study made by Corma et al. (2014) proved the high selectivity and stability of zirconium oxide, showing a deactivation of only 5%. They also concluded that zirconium oxide with platinum on alumina support was able to score higher conversion rates that other supports such as silica and activated carbon [29]. The same experiment was repeated varying different factors such as temperatures and types of catalyst. However, not a single experiment intended to study the same experiment in the liquid phase, therefore, no previous information was found concerning this experiment. Nevertheless, based on the experiments conducted in this field, it was found that metal oxides are of the most active catalysts for the ketonization reactions. The significance of the catalyst remains in its active sites, crystallinity, and structure [4].

CHAPTER III

EXPERIMENTAL PROCEDURE

A. Materials

Cerium nitrate hexahydrate $Ce(NO_3)_3.6H_2O$ and zirconium(IV) oxychloride octahydrate $ZrOCl_2.8H_2O$ were purchased from Sigma Aldrich, while ammonia (25 % in water) was purchased form VWR chemicals, and they were all used without any further purification for the catalysts preparation. Valeric acid (99.8 %) and 5-nonanone (98 %) were also bought from Sigma Aldrich and used as standards for GC-MS. Nitrogen gas was used for degassing of the acid used as a reactant.

B. Catalyst Synthesis

Cerium zirconium oxide was prepared by both wet impregnation and co-precipitation method based on the procedure mentioned by Sajith and Mohamed Jihad (2015) [30]. 0.1 M of aqueous solution of cerium nitrate and zirconium oxychloride was heated at 60°C for 15 minutes on a magnetic stirrer with hot plate. 25% of ammonia was added dropwise until the pH exceeded 10 and a yellowish precipitate is formed. The solution was stirred for 2 hours, and then the precipitate was collected, washed with water and acetone, dried for 8 hours in a vacuum oven at 60°C and calcined for 4 hours at different temperatures (400°C- 600°C and 800°C).

Zirconium dioxide was prepared only by co-precipitation method following the procedure described above.

C. Ketonization Experiment

The procedure for the ketonization experiment is described by Wu, et al. (2017) [31, 32]. A 100 ml Parr 5500 steel batch reactor is purged with N_2 at least twice to ensure the removal of air. In order to prevent the water from vaporizing, the reactor is then pressurized with 3 MPa of the same gas, heated to 350 ºC while the real pressure is increased to 7 MPa, at which the water is at its liquid phase. 0.3 g of catalyst is introduced into the reactor with 30 ml of pentanoic acid with a stirring rate of 500 rpm, and the reaction is conducted for 6 hours. After cooling down the reactor, the catalyst is collected, washed with water, filtered and dried in an oven at 105ºC for further use. Two liquid samples are analysed using gas chromatography.

D. Catalyst Characterization

The characterization of the catalysts was performed using X-ray powder diffraction (XRD), Brunauer–Emmett–Teller (BET), Scanning Electron Microscopy (SEM) including the use of an Energy Dispersive X-Ray Analyser (EDX), and Differential Scanning Calorimetry (DSC) and Thermogravimetric Analysis (TGA).

X-ray diffraction was carried out using PANalytical X-ray diffractometer, equipped with PIXcel-1D detector operating with CuK_{α}=1.541874 Å (40 kV and 40 mA). Data were transferred to X'Pert data collector over an angle range of 5-90° with a step size of 0.0131° and an integration time of 58.395s.

The BET surface area was measured using QuantaChrome AS1Win™ - Autosorb 1 based on the isotherm of liquid nitrogen at 77.3K. The catalyst was degassed with nitrogen on 250°C for 6 hours before the analysis. The BET surface area was calculated

from the adsorption branches in the relative pressure range of 0.05-0.30. The average pore size and the pore volume were calculated using BJH method.

The morphology of the catalyst is detected using Hitachi-SU-70 field emission SEM operating at 5 kV. The composition is evaluated using Oxford instrument INCA X-max 50 mm^2 energy dispersive X-ray (EDX) operating at 15 kV.

Catalyst stability was tested simultaneously in a SETARAM TG/DTA-DSC, and data were displayed and analyzed using Labsys TG (TG-DSC 1600ºC). The sample was heated to 800ºC under N_2 flow at a rate of $10^{o}C.min^{-1}$.

XPS was performed using Kratos ULTRA spectrometer where the sample maintained at a temperature of 20-30 °C is radiated with mono Al K_{α} (1486.58 eV) having a pass energy of 160 eV for survey spectra and 20 eV for narrow regions. C 1 s line at 284.8 eV was taken as a charge reference for the calibration of the binding energies. A Shirely type background was adopted for the construction and peak fitting of synthetic peaks in narrow region spectra while the synthetic peaks were of a mixed Gaussian-Lorenzian type. Relative sensitivity factors used are from CasaXPS library containing Scofield cross-sections.

The identification of the reaction products was established by an Agilent technologies 5975C GC/MS using Agilent HP-5MS capillary column (30 m × 0.25 mm × 0.25 μm) at a temperature of 290 °C (6 °C ramp). The carrier gas was Helium and the column head pressure was maintained at 0.1 bar (10 kPa). The injector and detector temperatures were set at 250 and 275 °C, respectively, and the injection volume was 0.2 μL in splitless mode.

CHAPTER IV

RESULTS AND DISCUSSION

A. XRD

The XRD patterns of $CeZrO_x$ prepared by both wet impregnation and co-precipitation are presented in Fig. 8. The catalyst pattern matched the cerium dioxide pattern, the zirconium dioxide pattern, and the pattern of $Ce_{0.1}Zr_{0.9}O_2$ (cerium zirconium dioxide having 10 Ce/90 Zr). The peaks generated by the XRD are narrow and sharp, which confirms the crystalline structure of the catalyst. However, the catalyst obtained from impregnation was discarded upon the XRD results that revealed that the catalyst prepared by co-precipitation method matched better with the reference pattern.

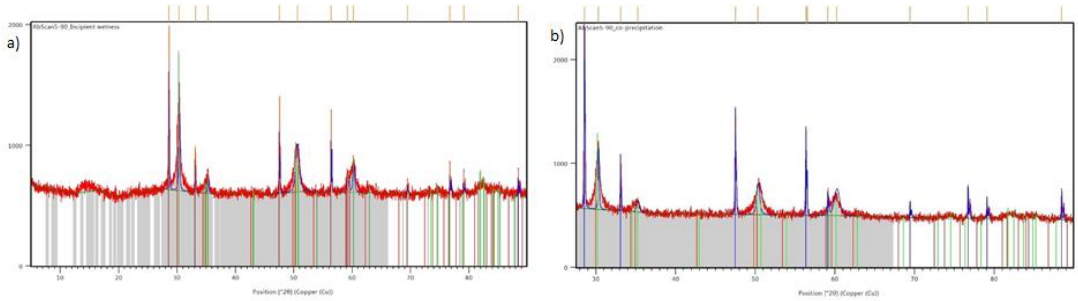

Figure 8: XRD pattern of the catalyst prepared by a) wet impregnation, b) co-precipitation

The following characterizations of the cerium zirconium dioxide catalyst were performed only on the catalyst resulting from co-precipitation.

The XRD patterns of the different zirconium dioxide prepared catalysts matched the reference pattern. Each one corresponds to a certain percentage of the crystal structure,

where Fig. 2-a is associated with the least crystalline (35%) and Fig. 2-c with the most crystal catalyst (89%). ZrO_2-400 appears to have a more amorphous structure than the ZrO_2-600, which is itself less crystalline than the ZrO_2-800. The difference in crystallinity percentages is related to the calcination temperature; as the temperature increases, the crystal formation is induced, and the monoclinic phase of the catalyst is more relevant. Moreover, there is a clear variability in the intensity of the peaks, they ranged from 500 counts in Fig.9-a to 1500 counts in Fig.9-b and further to 4000 counts in Fig.9-c. This is also linked to the crystallinity of the catalyst. The more crystalline the catalyst is, the higher the intensity of the peaks.

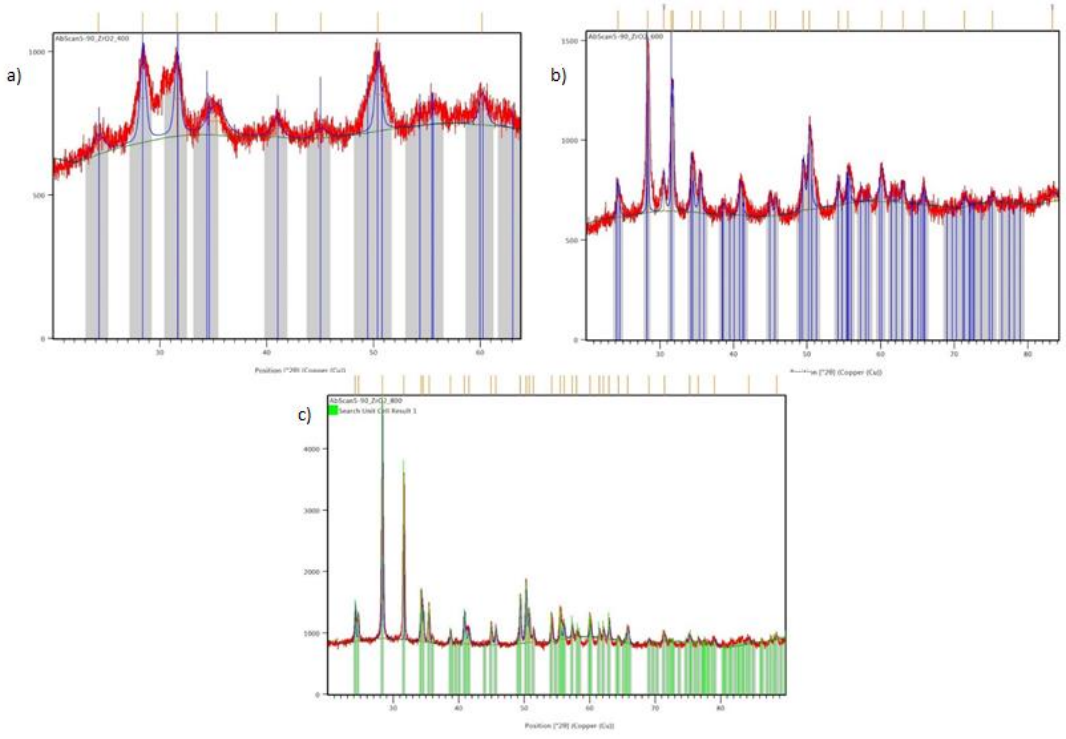

Figure 9: XRD patterns for a) ZrO2-400, b) ZrO2-600, and c) ZrO2-800

Table 1: The structural characteristics of ZrO_2 catalysts

Sample	Phase	Phase composition (%)
ZrO_2-400	Monoclinic	58
	Tetragonal	42
ZrO_2-600	Monoclinic	62
	Tetragonal	38
ZrO_2-400	Monoclinic	83
	Tetragonal	17

B. BET

The BET analysis of $CeZrO_2$ showed a surface area of 82.691 $m^2.g^{-1}$, matching perfectly the multi point BET isotherm, and a pore volume of 0.065 $cm^3.g^{-1}$. The obtained surface area was higher than the ones mentioned in the study of Oliveira, Garcia, Araujo, & Macedo (2012) [33], where the highest surface area acquired is about 42.3 $m^2.g^{-1}$.

As for ZrO_2 catalysts, the BET characterization of the catalysts revealed a strong effect of the temperature on the surface area obtained. A calcination temperature of 400°C resulted in a surface area of 153 $m^2.g^{-1}$, four times larger than the one obtained for a calcination temperature of 600°C and fifteen times larger than the one calcined at 800°C. As for the pore size, zirconium dioxide calcined at 400°C generates a smaller pore size compared to that obtained at 800°C, with an average of 60 Å and 390 Å respectively. The values obtained are compatible with the literature that relates a higher surface area with a smaller pore size. In the case of metal oxides, a higher surface area would contribute into a better interaction between the surface of the catalyst and the reactant.

Table 2: BET analysis of the prepared zirconium dioxide catalysts

	BET analysis	
Catalyst	Surface area (m^2/g)	Pore size (Å)
ZrO_2-400	153.434	60.433
ZrO_2-600	44.2254	167.432
ZrO_2-800	10.2558	388.741

C. SEM

SEM images of $Ce_{0.1}Zr_{0.9}O_2$ are presented in Fig.10. The smooth surface consists mainly of zirconium, while the small granules refer to the cerium element. However, the zirconium surface shows a homogeneous surface deprived from any kind of pores, where the cerium spheres are slightly separated which explains the surface area obtained in BET. It is also clear that the granules are vaguely distributed on the smooth plane zirconium surface. This theory is confirmed by the detailed analysis performed using EDX, which results are shown in table 3.

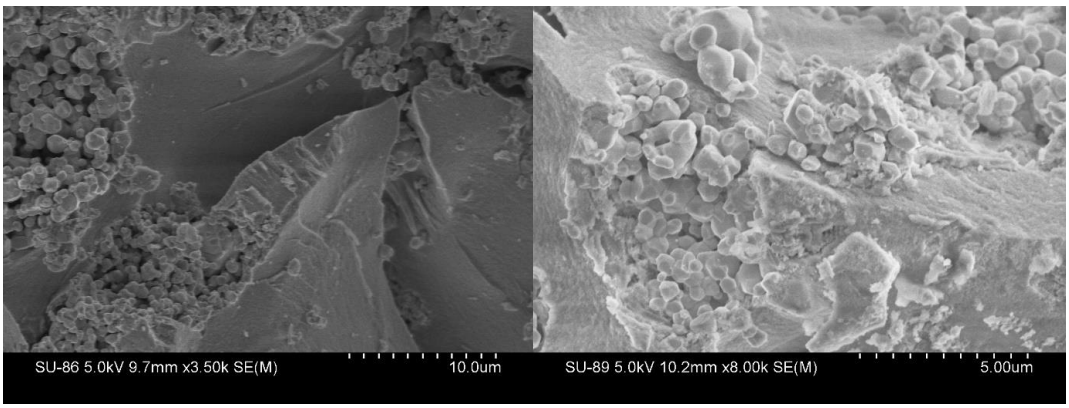

Figure 10: SEM images of the catalyst $CeZrO_2$

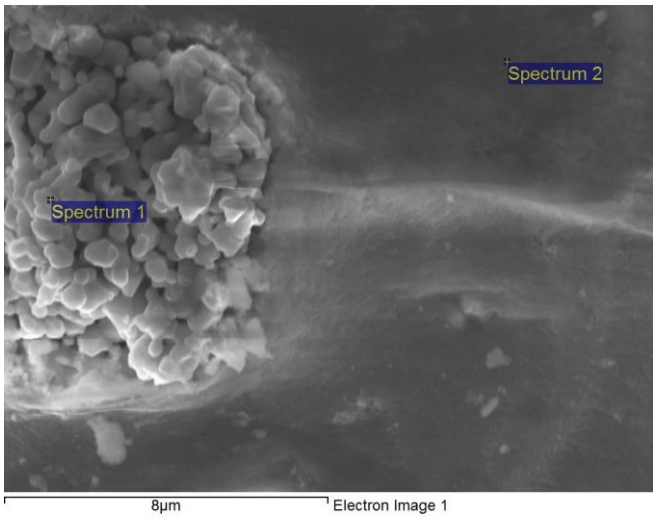

Figure 11: Magnified $CeZrO_2$ at 8 µm

The EDX analysis was focused on a magnified side of the above image as shown in Fig. 11, and the elemental analysis is shown in the following table.

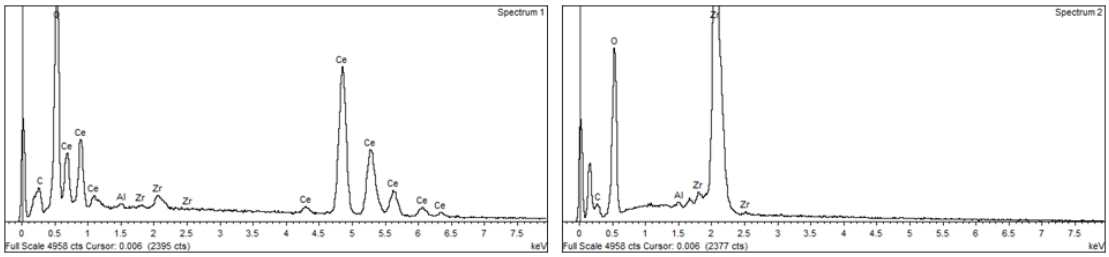

Figure 12: Element spectrum given by EDX.

Table 3: Elemental analysis of the catalyst

Spectrum	In stats.	C	O	Al	Zr	Ce
Spectrum 1	Yes	11.23	65.40	0.56	1.14	21.68
Spectrum 2	Yes	18.53	67.69	0.27	13.51	

All results in atomic%

The presence of carbon and aluminium is justififed by the choice of the carbon grid and the aluminium sample holder. The intensity of the beam was too high on that specific point that it crossed the sample into the grid and the holder.

As for the SEM analysis of ZrO_2, the photos below revealed a smooth outer surface of the catalysts with a visible porous medium on the inside. However, the shape of the pores was dependent of the calcination temperature as the difference between the surfaces of the catalysts is noticeable, where Fig. 13 displays remarkable location of porous medium, however, the surface shown in Fig. 14 is homogeneously smooth with little or no pores at all. The SEM analysis was complemented with an EDX testing to ensure that the surface of the catalysts consists only of zirconium and oxygen elements. Table 4 confirms the presence of Zr and O in different spectrums of both catalysts, spectrum 1-2 and 3-4 revealing the elements of ZrO_2-400 and ZrO_2-600 respectively.

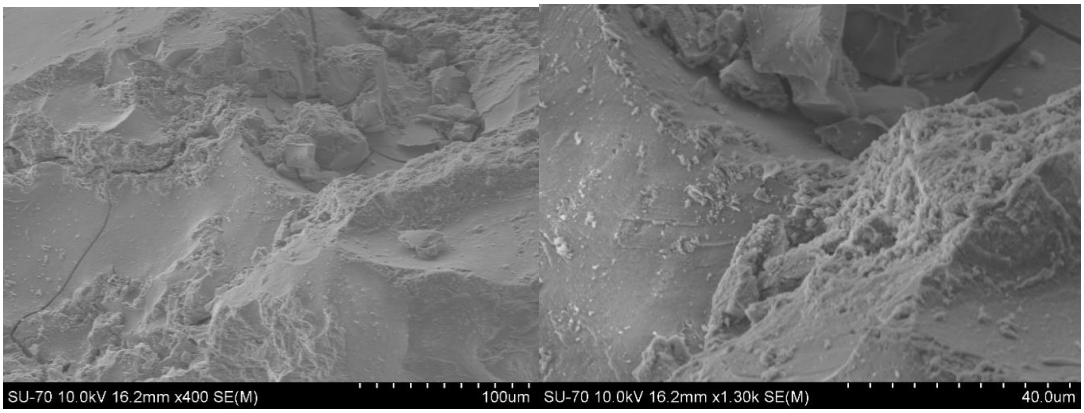

Figure 13: SEM analysis of ZrO2-400

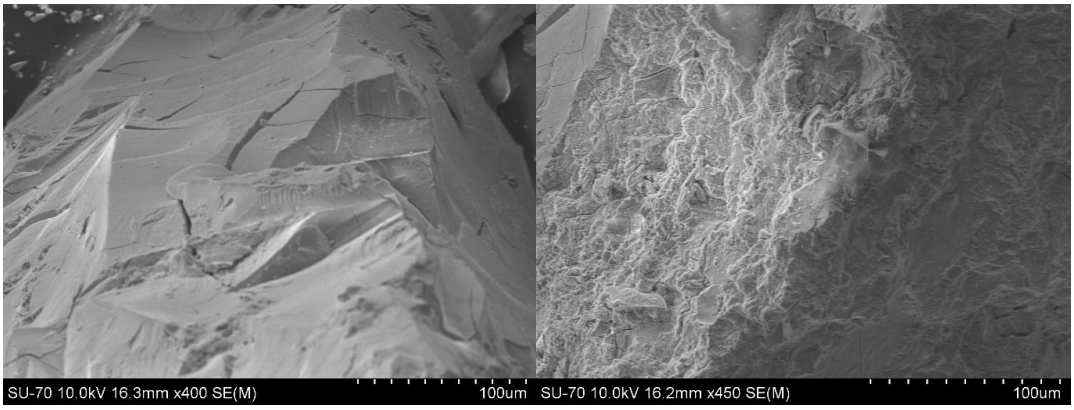

Figure 14: SEM photos of ZrO2-600

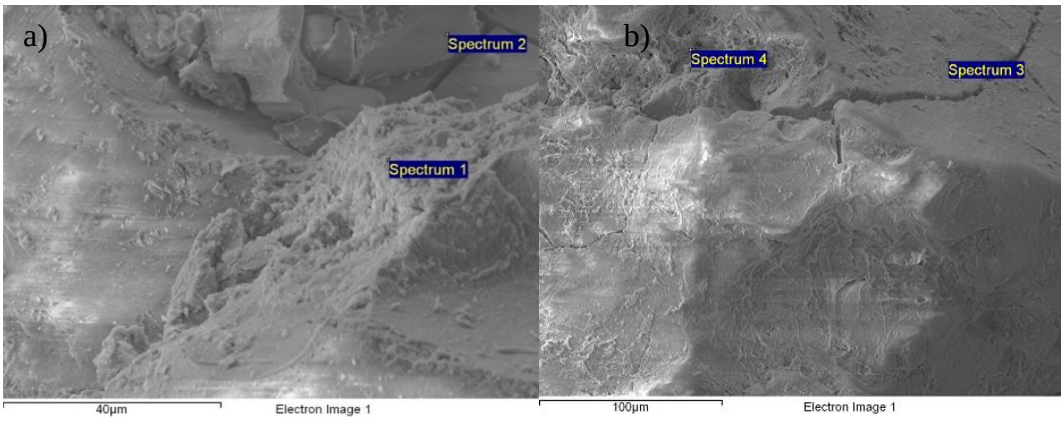

Figure 15: Magnified SEM photo of a) ZrO2-400 and b) ZrO2-600

Table 4: Elemental analysis showing the composition of the catalyst

Spectrum	In stats.	C	O	Zr	Total
Spectrum 1	Yes	8.85	33.28	57.87	100.00
Spectrum 2	Yes	11.65	31.53	56.82	100.00
Spectrum 3	Yes	18.56	32.29	49.15	100.00
Spectrum 4	Yes	6.20	26.54	67.26	100.00

All results in weight%

D. TGA

The thermal analysis of $CeZrO_2$ showed a minimal mass loss of order of 4.5% approximatly, which confirms the stability of the catalyst. The graph can be divided to two regions: the first region extends to a temperature of 100 °C where a rapid mass loss is occuring (2.5%), whereas the remaining 2% loss is partitioned on a range of temperatures extending from 100 to 800 °C.

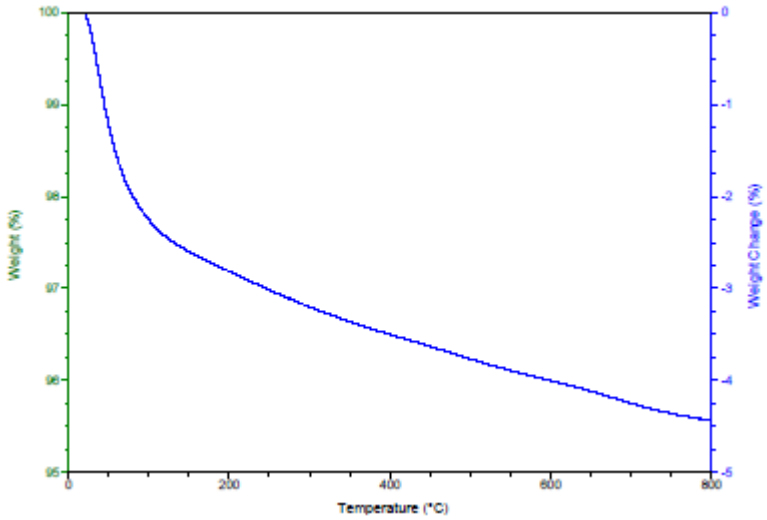

Figure 16: TGA pattern and analysis of $Ce_{0.1}Zr_{0.9}O_2$

The stability of three ZrO_2 catalysts was confirmed through a TGA analysis. As shown in Fig. 10 below, the weight loss scored a maximum of 5% for the ZrO_2-400 and a minimum of 0.35% for the ZrO_2-800. However, these ranges ensure the stability of the catalysts as no major weight loss was recorded. The dissimilarity emanates from the structure of the catalyst previously discussed. However, the graphs can also be separated into two regions: the rapid mass loss occurring at temperatures below 70 °C, whereas the remaining loss takes place at temperatures extending till 800 °C. One remarkable

point would be that the steepness of the mass loss in region one is proportional to the calcination temperature.

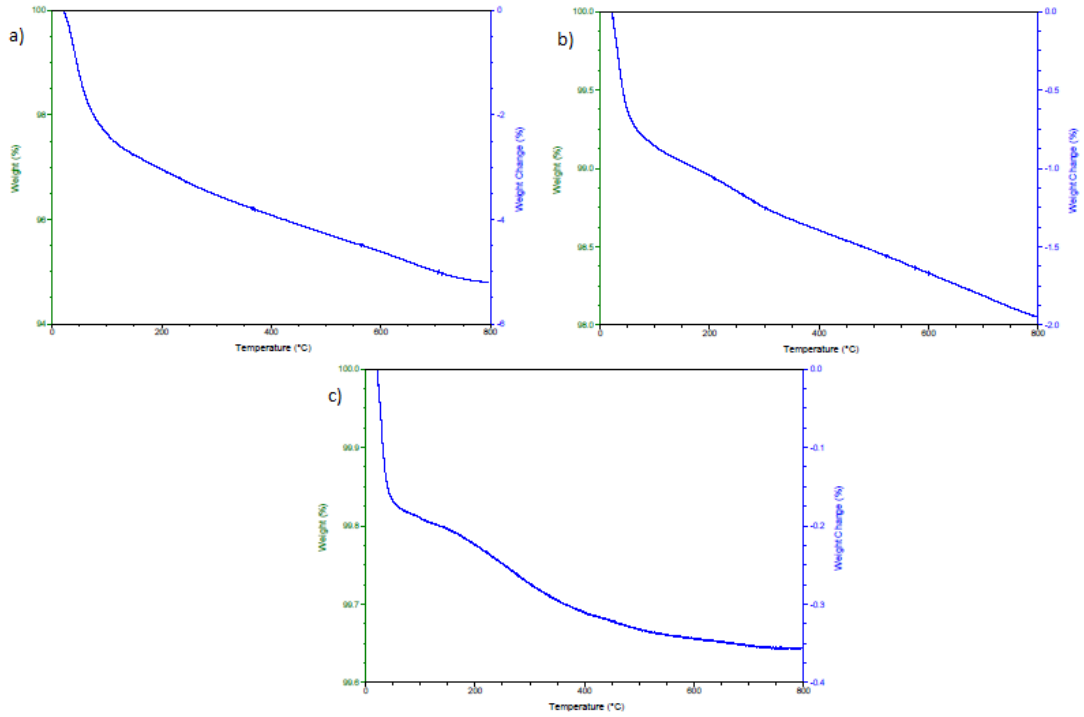

Figure 17: TGA analysis of ZrO2 calcined at a) 400°C, b) 600°C, and c) 800°C

E. Catalytic Ketonization in the liquid phase

The catalysts prepared were tested on different operating conditions taking into consideration the conservation of the liquid state of the water.

$CeZrO_2$ failed to produce any ketone under the conditions tested. The operating temperatures ranged from 150°C to 400°C, while applying the required pressure higher than the vapor pressure of water at this temperature to ensure that the water would stay in the liquid phase. The products obtained using this catalyst were analyzed using GC-MS, which confirmed the presence of pentane in all samples. Therefore, the $CeZrO_2$

promoted the decarboxylation of the acid into the corresponding alkane structure. The catalyst was collected after each experiment, washed and dried for a recycle run. The yield collected varied between 83.41% and 91.05%, which is considered a high recuperation percentage. The weight lost was compensated by fresh catalyst to maintain the conditions of the experiments that were repeated using the recycled catalyst. The results came out to prove that the catalyst incurred no deactivation in terms of activity, which is evident from the figure below (Fig. 18).

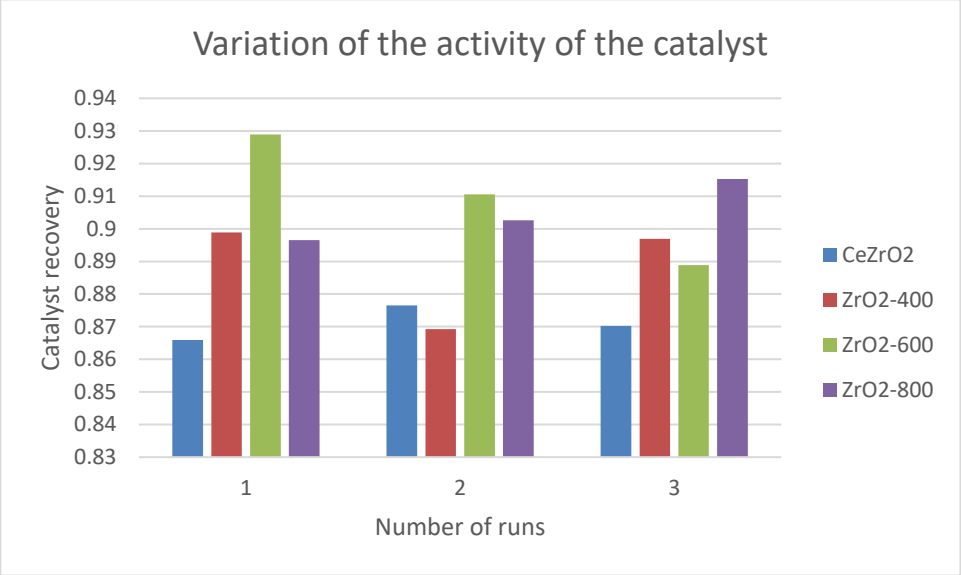

Figure 18: Catalyst recovery percentages

After the failure of the previous catalyst, the reaction was tested using zirconium dioxide catalysts calcinated at different temperatures (400, 600 and 800). Following the same procedure for all experiments, the liquid products were collected, separated from water by simple decantation and stored for further analysis. The catalysts were washed and dried as mentioned in the synthesis section. The mass of the catalyst lost was also

compensated with fresh catalyst, and the recycled catalyst was used in a second and a third run. The conditions under which the experiments took place figure in the table 4 below. The temperatures ranged between 150°C and 350°C, whereas the pressure was set to be 30 bar initially. The average yield of the recycled catalysts was 82.36%, scoring between 67.58% and 98.6%. None of the catalysts exhibited any sign of deactivation throughout the recycled runs. The lowest obtained yield of the organic compound was 88.98% while the highest was 96.13%, with an average of 94.16%. The different runs appear in the table 5 below showing the type of the catalyst used and the various operating conditions.

Table 5: Experiments made using ZrO_2 catalysts under different operating conditions

sample #	Name	Conditions (T-P)	Code	yield of organic products	yield of catalyst
1	ZrO2-400	150-30	Y-1	95.7	98.6
2	ZrO2-600	200-30	Y-2	96	73.9
3	ZrO2-800	220-30	Y-3	94.2	67.6
4	ZrO2 600	350-30	O-1	93.5	83
5	CeZrO2(b2)	320-25	O-2	95.2	86.7
6	ZrO2-800	150-30	O-3	89	77.9
7	ZrO2-600	150-30	O-4	93.7	80.1
8	ZrO2-800	350-30	O-5	96.1	79.4
9	ZrO2-800	320-30	O-6	93.7	85.9
10	2 wt% ZrO2 550 (NO3)2	350-30	Br-1	95.9	82.3
11	ZrO2-400	350-30	Bl-1	95.8	79.2
12	ZrO2-400	330-35	Bl-2	94.6	90.7
13	ZrO2-550	350-68	Bl-3	89.2	82.8
14	ZrO2(400)	350-30	Bl-4	93.8	88.4
15	ZrO2-400	320-30	Bl-5	96	79.2
			AVG	94.16	82.4

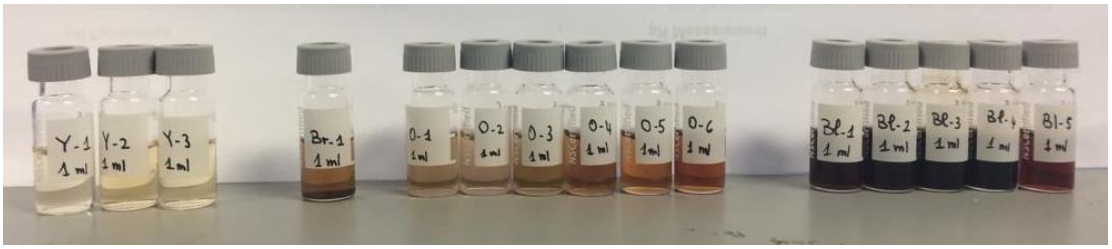

Figure 19: Liquid samples collected

The same sample was analyzed twice, with and without the addition of the internal standard; however, due to the reactivity of the ISTD with the liquid product, the compounds obtained will not be mentioned. All compounds detected by the GS-MS figure in the following table 5. Some of them were remarkable such as 2-hexanone, ammonia, gamma-valerolactone or 4,5-Dihydro-5-methyl-2(3H)-furanone, and xylose. The 5-nonanone ketone, desired product intended in this experiment, was detectable in different samples, deprived from ISTD addition. 5-nonanone was present in 5 samples noted Bl-1, Bl-2, Bl-3, Bl-4 and Bl-5. One finding was also the detection of the ketene inside the liquid product. The ketene is supposed to be an intermediate of the ketonization experiment as previously discussed. An intermediate is a compound that forms from the reactants and reacts further to give the product. In other words, an intermediate cannot be detected at the end of an experiment, which leads to the continuous debate whether to consider the ketene as an intermediate or as a by-product. The result obtained for some of the samples challenges the hypothesis of the intermediate and to support the supposition of a by-product. Moreover, the 2-hexanone identified in some of the samples might actually be a product, or a result from the β-scission of the 5-nonanone. However, it is not possible to confirm one assumption or refute the other.

Table 6: Some obtained compounds

4,5-Dihydro-5-methyl-2(3H)-furanone	Butane
1,4,7,10,13,16-Hexaoxacyclooctadecane	Hexanoic acid
2-Hexanone	Pentanoic acid
2-Octene, (Z)-	Propanedioic acid, propyl-
Ammonia	Valproic Acid
1-Butene	5,6-Decanedione
1-Heptene ; 2-Heptene ; 3-Heptene, (E)- ; 3-Heptene, (Z)-	5-Nonanone
1-Pentanol, 2,2-dimethyl-	Acetic acid ; Acetic acid, 2-methylpropyl ester
1-Propanol, 2-amino-	Butanamide
2-Hexene, (Z)- ; 3-Hexene, (E)-	Butanoic acid, (n- ; 2-methyl- ; 3-methyl- , 2-methylpropyl ester ; 3-methyl-, butyl ester)
2-Pentenoic acid ; 4-Pentenoic acid	cis-2-Nonene
3-Ethylheptanoic acid	Heptanoic acid ; Nonanoic acid ; Octanoic Acid ; Propanoic acid
3-Hexenoic acid, (E)- ; 4-Hexenoic acid	Pentanoic acid, (1-methylpropyl ester ; 1-methylethyl ester ; 2-methylpropyl ester ; 4-oxo- ; butyl ester)
3-Methoxy-2-methyl-1-pentene	Xylose
4-Methyloctanoic acid	Ketene

F. XPS

In order to confirm the success of ZrO_2-400 compared to the two other catalysts, an XPS analysis was made to depict any differences on the surface of the prepared catalysts.

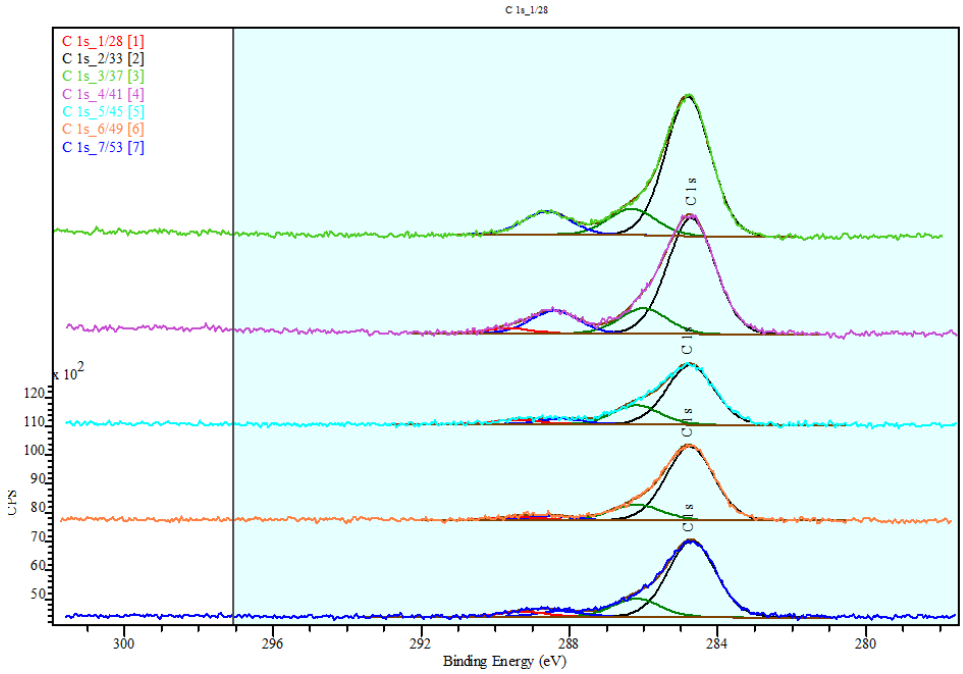

Figure 20: C 1s XPS spectrum of the different fresh and used catalysts

Figure 20 displays the XPS spectrum of the carbon element on each of the catalyst surfaces ordered as follows: ZrO_2-400 used, ZrO_2-550 used, and fresh ZrO_2-400, 600 and 800 respectively. The first two spectra exhibit similar behavior, whereas the last three spectrums, different form the previous two, look the same. The five spectrums reveal the presence of three peaks corresponding to a binding energy of 284.8 eV (C-C), 286 eV (C-O) and 288.5 eV (C=O) respectively, which indicates a high surface reactivity. However, it is clear that the intensity of the peaks corresponding to 286 eV and 288.5 eV is higher in the first two spectrums compared to the following three, indicating the presence of ketone groups and hydrocarbons on the surface of the used catalysts and their absence on the fresh ones. A sp^3 carbon state is evident to be absent in all five catalysts.

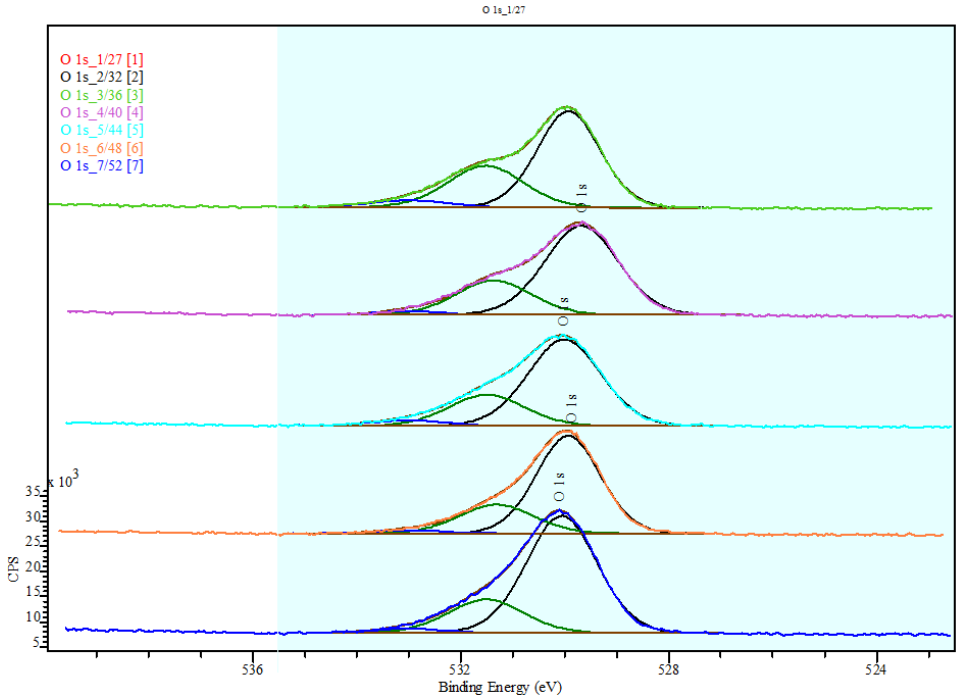

Figure 21: O 1s XPS spectrum of the different fresh and used catalysts

Concerning the oxygen spectrum, the major peak is located at a binding energy of 530 eV corresponding to a metal oxide state. This is explained by the fact that the catalysts analyzed are all zirconium dioxide. Moreover, in the first two spectrum (used ZrO_2), a shoulder with a binding energy of 531.1-532 eV is present, indicating the presence of an organic C-O bond. The presence of this shoulder can be explained by the deposition of potential hydroxyl groups on the surface of the catalysts. In addition to the shoulder, a minor peak is present at a binding energy of 533 eV which is in direct relation with the presence of a C=O group, a supplement proof of the formation of the ketone.

The elemental composition of each of the fresh catalysts is mentioned in the table below.

Table 7: XPS analysis of the three different catalysts

	ZrO2-400				ZrO2-600				ZrO2-800			
Name	Pos.	FWHM	Area	At%	Pos.	FWHM	Area	At%	Pos.	FWHM	Area	At%
C 1s	283.72	3.176	2885.1	12.22	284.58	3.308	2764	10.46	284.6	3.522	4797.03	15.99
O 1s	529.72	3.344	38771.61	56.06	529.58	3.489	44083.32	56.94	529.6	3.357	45553.55	51.84
Zr 3d	181.72	4.649	51718.1	31.12	182.58	4.804	57382.18	30.85	181.6	4.77	63681	30.16
Cl 2s	267.72	2.946	240.32	0.6	268.58	5.375	782.9	1.75	269.6	3.654	1017.52	2.01

There is no major difference in the composition of the surface of the three catalysts. However, a slight difference in oxygen element percentages resides between ZrO_2-400, 600 and ZrO_2-800, compensated by higher C- and Cl- percentages in the latter catalyst compared to the former ones. In general, the catalyst showed a similar composition of the surface.

Another analysis was made for the successful catalyst to try to prove any differences between the fresh one and the used one after a first run of the experiment. The data figures in the table below.

Table 8: Comparison between the fresh and the used ZrO2-400

	fresh ZrO2-400				Used ZrO2-400			
Name	Pos.	FWHM	Area	At%	Pos.	FWHM	Area	At%
C 1s	283.72	3.176	2885.1	12.22	284.55	3.306	6332.42	22.8
O 1s	529.72	3.344	38771.61	56.05	529.55	3.595	41302.37	50.75
Zr 3d	181.72	4.649	51718.1	31.12	181.55	4.624	51713.47	26.45

The atomic percentage of the carbon element has increased by 10% after the first round of experiments, whereas the percentages of oxygen and zirconium have slightly decreased by 5-6% which is resulting from the release of water and CO_2. The presence of carbon products reduced the composition of ZrO_2 compared to the fresh catalysts. A

more detailed analysis of the signals depicted the presence of hydrocarbon content, and carboxyl/ester groups, which presence is already proven by the GC analysis of the liquid products. The highest peak among the carbon element relates to the presence of ketone groups with an atomic percentage of 15.5% out of the total 22.8%, previously demonstarted by the spectrums. This might give us an approximation of the yield of ketones, which would be 67.9%.

CHAPTER V

CONCLUSION

The ketonization of pentanoic acid in liquid phase lead to the formation of 5-nonanone, which upon hydrogenation, is transformed to nonane, a biofuel additive. The experiment took place under a 350ºC temperature and a pressure of 30 bar, using $CeZrO_2$ and ZrO_2 as catalysts. The former catalyst turned out to be unsuccessful for this experiment, whereas the success of the latter one was highly dependent on the calcination temperature. A high calcination temperature resulted in a low porosity catalyst, inhibiting its activity on the conversion of the acid. The most convenient catalyst turned out to be ZrO_2 calcined at 400ºC, recording the highest surface area of 150 $m^2.g^{-1}$. However, the catalysts showed no sign of deactivation throughout the recycle runs. GC-MS confirmed the feasibility and the success of this experiment, by depicting the 5-nonanone in 5 samples of the liquid product collected. The XPS confirmed that this experiment takes place on the surface of the catalyst and does not interfere with the bulk of it, it also proved the presence of the ketones on the surface of the catalyst with a percentage of 70%. The liquid phase ketonization was proved possible in this work; however, further optimization of the operating conditions and the choice of catalyst might be necessary. Another alternative would be the direct conversion of valeric acid to nonane without the formation the ketone, using palladium-based catalyst under H_2 flow.

REFERENCES

1. Administration, U.E.I., *International Energy Outlook 2017*. 2017.
2. Neumann, G.T., D. Garcia, and J.C. Hicks, *Catalysts for Biofuels*, in *Heterogeneous Catalysis at Nanoscale for Energy Applications*, F.F. Tao, W.F. Schneider, and P.V. Kamat, Editors. 2015, John Wiley & Sons, Inc.
3. Biofine Hydrolysis Process and Derivative Product Upgrading Technologies, in Water for Energy and Fuel Production. p. 183-203.
4. Pham, T.N., et al., Ketonization of Carboxylic Acids: Mechanisms, Catalysts, and Implications for Biomass Conversion. ACS Catalysis, 2013. **3**(11): p. 2456-2473.
5. Pulido, A., et al., Ketonic decarboxylation reaction mechanism: a combined experimental and DFT study. ChemSusChem, 2013. **6**(1): p. 141-51.
6. Schlaf, M. and Z.C. Zhang, Reaction pathways and mechanisms in thermocatalytic biomass conversion I. 2016-2015, DE: Springer Verlag.
7. McMurry, J., *Fundamentals of organic chemistry*. seventh ed. 2010, Stamford, CT: Cengage Learning Publisher.
8. Neunhoeffer, O. and P. Paschke, *Über den mechanismus der ketonbildung aus carbonsäuren.* Berichte Der Deutschen Chemischen Gesellschaft (A and B Series), 1939. **72**(4): p. 919-929.
9. Pestman, R., et al., Reactions of carboxylic acids on oxides .2. bimolecular reaction of aliphatic acids to ketones. Journal of Catalysis, 1997`. **168**(2): p. 265-272.

10. Nagashima, O., et al., *Ketonization of carboxylic acids over CeO2-based composite oxides.* Journal of Molecular Catalysis a-Chemical, 2005. **227**(1-2): p. 231-239.

11. Ignatchenko, A.V., Density Functional Theory Study of Carboxylic Acids Adsorption and Enolization on Monoclinic Zirconia Surfaces. The Journal of Physical Chemistry C, 2011. **115**(32): p. 16012-16018.

12. Pham, T.N., et al., Aqueous-phase ketonization of acetic acid over Ru/TiO2/carbon catalysts. Journal of Catalysis, 2012. **295**: p. 169-178.

13. Staudinger, H., *Ketene, eine neue Körperklasse.* Berichte der Deutschen Chemischen Gesellschaft, 1905. **38**(2): p. 1735-1739.

14. González, F., G. Munuera, and J.A. Prieto, *Mechanism of ketonization of acetic acid on anatase TiO2 surfaces.* Journal of the Chemical Society, Faraday Transactions 1: Physical Chemistry in Condensed Phases, 1978. **74**: p. 1517.

15. Randery, S., J. Warren, and K. Dooley, *Cerium oxide-based catalysts for production of ketones by acid condensation.* Applied Catalysis a-General, 2002. **226**(1-2): p. 265-280.

16. Dooley, K., et al., Ketones from acid condensation using supported CeO2 catalysts: Effect of additives. Applied Catalysis a-General, 2007. **320**: p. 122-133.

17. Hendren, T. and K. Dooley, Kinetics of catalyzed acid/acid and acid/aldehyde condensation reactions to non-symmetric ketones. Catalysis Today, 2003. **85**(2-4): p. 333-351.

18. Sanati, M., et al., *Catalysis*. Vol. 17. 2004, Cambridge, U.K.: Royal Society of Chemistry.

19. Pestman, R., et al., Reactions of carboxylic acids on oxides .1. selective hydrogenation of acetic acid to acetaldehyde. Journal of Catalysis, 1997. **168**(2): p. 255-264.

20. Martinez, R., M. Huff, and M. Barteau, *Ketonization of acetic acid on titania-functionalized silica monoliths.* Journal of Catalysis, 2004. **222**(2): p. 404-409.

21. Kim, K.S. and M.A. Barteau, Structure and composition requirements for deoxygenation, dehydration, and ketonization reactions of carboxylic acids on TiO 2(001) single-crystal surfaces. Journal of Catalysis, 1990. **125**(2): p. 353-375.

22. Bettelheim, F., et al., *Introduction to organic and biochemistry*. nineth ed. 2010, Belmont CA: Thomson Brooks/Cole.

23. Ignatchenko, A. and E. Kozliak, Distinguishing enolic and carbonyl components in the mechanism of carboxylic acid ketonization on monoclinic zirconia. Acs Catalysis, 2012. **2**(8): p. 1555-1562.

24. Kuriacose, J.C. and S.S. Jewur, *Studies on the surface interaction of acetic acid on iron oxide.* Journal of Catalysis, 1977. **50**(2): p. 330-341.

25. Rajadurai, S. and J.C. Kuriacose, Catalytic Activity of the 1:1:1 Zn, Cr and Fe Mixed Oxide: Mechanistic Study of the Ketonization of Acetic Acid. Materials Chemistry and Physics, 1986. **16**(1): p. 17-29.

26. Pestman, R., et al., The formation of ketones and aldehydes from carboxylic acids, structure-activity relationship for two competitive reactions. Journal of Molecular Catalysis. A, Chemical, 1995. **103**(3): p. 175-180.

27. Bamberger, E., Berichte Der Deutschen Chemischen Gesellschaft. 1910. **43**(3): p. 3917.

28. Zaytseva, Y.A., et al., Effect of Gas Atmosphere on Catalytic Behaviour of Zirconia, Ceria and Ceria–Zirconia Catalysts in Valeric Acid Ketonization. Topics in Catalysis, 2013. **56**(9-10): p. 846-855.

29. Corma, A., et al., Conversion of levulinic acid derived valeric acid into a liquid transportation fuel of the kerosene type. Journal of Molecular Catalysis A: Chemical, 2014. **388-389**: p. 116-122.

30. Sajith, V. and P. Mohamed Jihad, Development of stable cerium zirconium mixed oxide nanoparticle additive for emission reduction in biodiesel blends. Research & Reviews: Journal of Engineering and Technology, 2015. **4**(2).

31. Wu, K., et al., Aqueous-phase ketonization of acetic acid over Zr/Mn mixed oxides. AIChE Journal, 2017. **63**(7): p. 2958-2967.

32. Wu, K., et al., *Carbon Promoted ZrO2 Catalysts for Aqueous-Phase Ketonization of Acetic Acid.* ACS Sustainable Chemistry & Engineering, 2017. **5**(4): p. 3509-3516.

33. Oliveira, C.F., et al., Effects of preparation and structure of cerium-zirconium mixed oxides on diesel soot catalytic combustion. Applied Catalysis A: General, 2012. **413-414**: p. 292-300.